J Mater Sci (2008) 43:6376–6384
DOI 10.1007/s10853-008-2559-4

Preparation of nano-grained zirconia ceramics by low-temperature, low-pressure spark plasma sintering

Michihito Muroi · Geoff Trotter · Paul G. McCormick · Masakazu Kawahara · Masao Tokita

Received: 30 November 2007 / Accepted: 14 February 2008 / Published online: 13 July 2008

Abstract Ce- and/or Y-doped zirconia nanopowders having average particle sizes ranging 12–18 nm have been synthesized by a technique based on mechanochemical processing (MCP). Despite their small particle size, the powders had excellent compactibility with green densities exceeding 50% achieved under a moderate uniaxial pressure of 150 MPa. Nearly fully dense ceramics having grain sizes of around 100 nm were successfully produced from these powders by spark plasma sintering (SPS) at temperatures of 1,050–1,150 °C for 5 min under pressures of 50–80 MPa; these temperatures and pressures are considerably lower than those required for achieving near full density with conventional nanopowders. Hardness and fracture-toughness measurements showed that the ceramics prepared by SPS had superior mechanical properties to those prepared by conventional pressureless sintering. It is argued that the high sinterability of the MCP nanopowders is ascribed to their ability to form uniform powder compacts under relatively low pressure, and that that ability in turn originates in two features of the MCP powders: absence of hard agglomeration and pseudo-spherical particle morphology.

Introduction

Zirconia nanopowders and their sintering behavior have been extensively investigated for decades, aimed at lowering sintering temperature and producing fine-grained ceramics [1–6]. It has been demonstrated that the use of nanopowders enables the sintering temperature to be lowered significantly, from 1,400 to 1,500 °C, typical sintering temperatures for sub-micron powders now commercially available, down to around 1,050 °C, or even 950 °C if sintering is carried out in a vacuum or inert atmosphere [1–6]. Nevertheless, nanopowders are not currently used for mass production of zirconia ceramics. The primary reason for this is that in general low temperature sintering is achieved only when the powders are consolidated under exceedingly high pressures, ranging from around 500 MPa to 3 GPa [2–6], or with special methods such as centrifuge casting [1]. The necessity of high pressure to prepare sinterable green bodies not only increases the capital and maintenance costs of pressing equipment, but also limits the size of green bodies that can be produced by simple dry pressing; being expensive and having a low production rate, a process like centrifuge casting is generally not suitable for mass production of ceramics.

Exceptions to the above are zirconia nanopowders we have recently developed, which can be sintered to near full density at temperatures in the range 1,100–1,200 °C even when they are consolidated under a moderate uniaxial pressure of the order of 100 MPa [7]. These powders were synthesized by a technique based on mechanochemical processing (MCP) [8, 9], which has proven to be effective in producing agglomerate-free nanopowders of a variety of materials, including transition metals [10], oxide ceramics [11–14], sulfide semiconductors [15], and various kinds of magnetic materials [16–18].

On the processing side, spark plasma sintering (SPS) has proven to be effective in producing high-density ceramics at a lower temperature in a much shorter time than conventional pressureless sintering. SPS is a pressure-assisted

M. Muroi (✉) · G. Trotter · P. G. McCormick
Advanced Nanotechnology Limited, 108 Radium Street, Welshpool, WA 6106, Australia
e-mail: michi.muroi@advancednanotechnology.com

M. Kawahara · M. Tokita
SPS Syntex Inc., 509 West KSP Kanagawa Science Park, 3-2-1 Sakado, Takatsu-ku, Kawasaki-shi, Kanagawa 213-0012, Japan

sintering method, but unlike conventional hot pressing, heating is effected by a high-intensity, low-voltage dc pulsed electric current passed directly through the sample (if electrically conducting) and through the mold typically made of graphite. Its application to zirconia nanopowders has been studied extensively, but the published results [19–24] show that a temperature of around 1,300 °C is still needed to achieve near full density under a moderate pressure of below ~100 MPa, a pressure that can be accessed relatively easily in a typical experimental or production setup.

With this background in mind, we have carried out SPS experiments using our zirconia nanopowders and demonstrated that they can be sintered to near full density at significantly lower temperatures than conventional nanopowders. We have characterized the structural, microstructural and mechanical properties of the sintered ceramics, which are presented and discussed in this article.

Experimental

Four types of zirconia nanopowders, having various particle sizes and compositions as listed in Table 1, were synthesized by a two-step process, consisting of (1) the preparation of undoped zirconia nanoparticles by MCP and (2) the addition of stabilizing agents by precipitation.

The raw materials used for preparing undoped zirconia were dried $ZrOCl_2$ and NaCl. The two compounds, mixed in various ratios, were loaded in an attrition mill containing zirconia grinding media, and milled for 1 h. The milled powder, composed of $ZrOCl_2$ and NaCl in the form of a nanocomposite, was heat treated in air to form zirconia nanoparticles embedded in a salt matrix. Since the nanoparticles formed were separated by a diluent phase, coarsening, sintering and agglomeration were effectively prevented. The powder was subsequently washed with deionized water to remove NaCl. The resultant zirconia nanoparticles were kept in slurry form for further processing.

As can be seen in the transmission electron microscopy (TEM) image shown in Fig. 1, the nanoparticles are pseudo-spherical, have a relatively broad size distribution, and are free of hard agglomeration. The average particle size was in the range 12–18 nm, depending on the synthesis conditions.

In the second step, the zirconia nanoparticles were first dispersed in water at pH ~ 2. To the dispersion was added a solution of $CeCl_3$ and/or YCl_3 as a precursor to a stabilizing agent; in one instance, a solution of $Al_2Cl_4(OH)_2$ and $FeCl_3$ was also added to prepare a powder doped with Al and Fe. The pH of the dispersion was then slowly increased to ~10.5 by adding ammonia solution to induce precipitation of the stabilizing agent. The precipitate, a mixture of the zirconia nanoparticles and the stabilizing agent, was washed and dried at about 80 °C. The as-dried precipitate was in the form of friable chunks, which were gently ground into powder with a mortar and pestle.

As observed in the TEM image presented in Fig. 2a, the powders thus prepared consist of spherical primary particles densely packed into agglomerates, which are "soft" agglomerates, since no high-temperature processing is involved after crystalline zirconia nanoparticles are formed in step 1. As discussed later, this is a key attribute that makes the powders highly sinterable. Elemental mapping by means of electron-energy-loss spectroscopy (EELS) shows that the stabilizing agent is intimately mixed with zirconia nanoparticles, and that the former tends to coat the latter; see Fig. 2b. In the following discussions, those powders which were prepared by the method described above are referred to as MCP powders.

Table 1 SPS conditions and density of sintered ceramics

Powder		Sintering conditions					Relative density of ceramic (%)
Composition (mol% additive)	Particle size (nm)	Sample diameter (mm)	Heating rate (°C/min)	Temperature[a] (°C)	Hold time (min)	Pressure[b] (MPa)	
2.4% Y_2O_3	13.0	10	100	1,100	5	50	96.4
		30	100	1,100	5	50	86.4
		30	100	1,150	5	70	99.2
2.4% Y_2O_3	18.0	10	100	1,100	5	50	97.5
4% CeO_2 + 1% Y_2O_3	12.3	10	200	700	0	50	55.0
		10	200	1,100	0	50	79.8
		10	100	1,100	5	50	91.5
9% CeO_2 + 2% Al_2O_3 + 0.5% Fe_2O_3	15.2	10	100	1,050	5	80	98.9

[a] Temperature measured using a thermocouple inserted into the graphite mold

[b] Pressure applied prior to heating and released prior to cooling

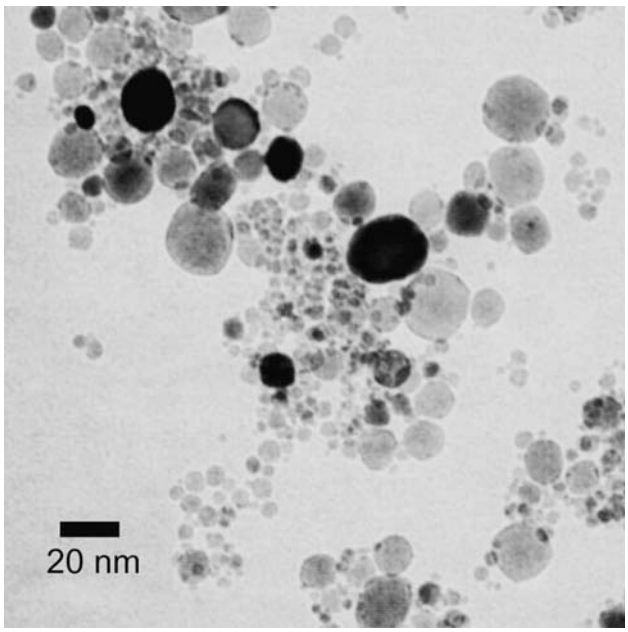

Fig. 1 TEM image of zirconia nanoparticles prepared by MCP

In the SPS experiments, SPS Syntex model SPS-511S or SPS-2040 was used depending on sample size. The sintering conditions, summarized in Table 1, are typical of preparing zirconia ceramics by SPS, except for the lower temperatures. The sintered ceramics were heat treated in air at 900 °C for 2 h in a furnace. The heat treatment turned the color of the ceramics from gray to blackish (because of carbon contamination and/or oxygen vacancies) into whitish to light brown (because of iron impurity or additive).

The ceramics were characterized for density (determined by the Archimedes method for high-density samples or from the weight and external dimensions for low-density samples), crystal structure and phases present [by X-ray diffraction (XRD)] and microstructure [by scanning electron microscopy (SEM)].

The Vickers hardness (H_V) and fracture toughness (K_{IC}) were measured using a standard indentation technique. A load of 50 kg was applied to a polished surface of a sintered pellet for 15 s to make an indent. The H_V was calculated on the basis of the equation $H_V = 1.854P/a^2$, where P is the load and a is the diagonal length of the indent. The K_{IC} was derived using the equation $K_{IC} = 9.052 \times 10^{-3} \cdot H_V^{3/5} \cdot E^{2/5} \cdot a \cdot c^{-1/2}$, where E is Young's modulus assumed to be 200 GPa, a is the diagonal length of the indent, and c is the crack length [25].

Results and discussion

The densities of the sintered ceramics are listed in the last column of Table 1. These data show that the density is very sensitive to sintering temperature, holding time and pressure. Particularly noteworthy is the fact that near full density is achieved at 1,100 °C under 50 MPa for the powders doped with Y_2O_3 (Y-powders hereafter), and at 1,050 °C under 80 MPa for the powder doped with CeO_2 and small amounts of Al_2O_3 and Fe_2O_3 (C-powder hereafter). These temperatures and pressures are significantly lower than those needed to achieve near full density with conventional nanopowders; this is seen clearly in Fig. 3, where the temperature–pressure combinations needed to achieve a density greater than 95% are plotted for MCP and conventional zirconia nanopowders. Near full density was not achieved for the powder doped with CeO_2 and Y_2O_3 (CY-powder hereafter) under the conditions used (1,100 °C and 50 MPa); however, in view of the strong temperature and pressure dependence of the density observed for the Y-powders, near full density is expected to be achieved by slightly increasing temperature and/or pressure.

X-ray diffraction measurement indicated that the ceramics made from the Y- and CY-powders consisted almost entirely of tetragonal zirconia. On the other hand,

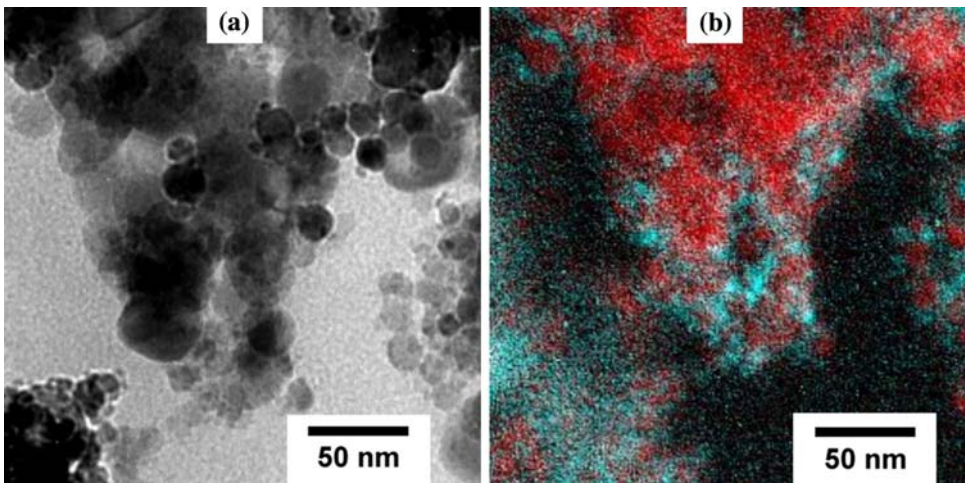

Fig. 2 (**a**) TEM image of Ce-doped zirconia powder. (**b**) Elemental map of the same region. Red denotes zirconium and blue, cerium

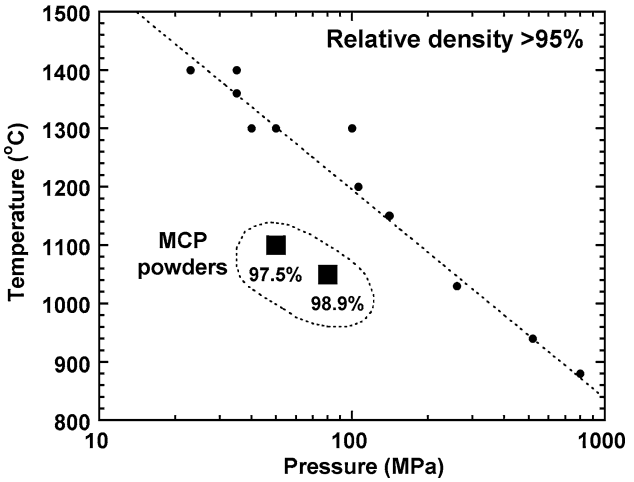

Fig. 3 Temperature–pressure combinations required to prepare nearly fully dense zirconia ceramics by SPS. Large squares are for MCP nanopowders, and small circles for conventional nanopowders (data from [19–23])

the ceramic made from the C-powder was found to contain significant amounts of monoclinic zirconia and a solid solution of the type $(Zr_{1-x}Ce_x)O_2$ ($x \sim 0.5$), in addition to tetragonal zirconia. (The coexistence of monoclinic zirconia and a solid solution containing a high concentration of ceria implies incomplete compositional homogenization as a result of the high heating rate and low sintering temperature.) The dominance of monoclinic zirconia and the presence of the ceria-rich solid solution, however, seem to be limited to thin layers near the surface; XRD measurement on a surface after polishing or on a cross-section has revealed the dominance of tetragonal zirconia (>90%) over monoclinic, with no indication of the presence of the ceria-rich solid solution.

Scanning electron microscopy images of fracture surfaces of ceramics made from Y- and C-powders are presented in Figs. 4–6. All the samples have dense, reasonably uniform, fine-grained microstructure with an average grain size of around 100 nm. The appearance of the surface suggests intergranular fracture.

Figure 7 shows SEM images of fracture surfaces of ceramics made from the CY powder. The three samples, subjected to SPS under different conditions, had densities varying over a wide range between 55 and 92%. Two features are noticed. First, no abnormal grain growth is observed, despite the broad particle size distribution of the starting powder. In fact, the size distribution seems to narrow down as densification proceeds. Second, despite the marked increase in density with increasing temperature or holding time, grain growth is insignificant. This is presumably due to the very high heating rate, which allows the system to quickly pass the temperature range in which coarsening through surface diffusion dominates over densification through bulk diffusion.

The variation of the H_V with density is shown in Fig. 8 for ceramics made from the Y-powders. A clear tendency is observed that the hardness increases with density.

The K_{IC} versus H_V relationship is shown in Fig. 9 for a larger number of nearly fully dense tetragonal zirconia polycrystals (TZPs) made from MCP nanopowders

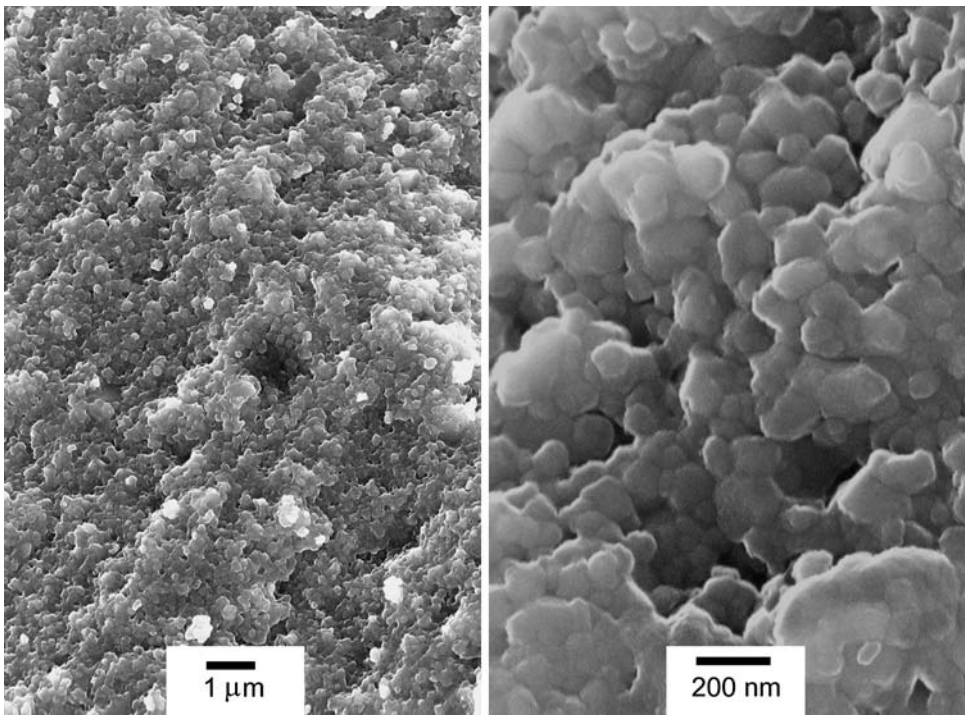

Fig. 4 SEM images of fracture surfaces of a ceramic (10 mm in diameter) made from 18 nm zirconia nanopowder doped with 2.4% Y_2O_3. Sintered at 1,100 °C for 5 min under 50 MPa

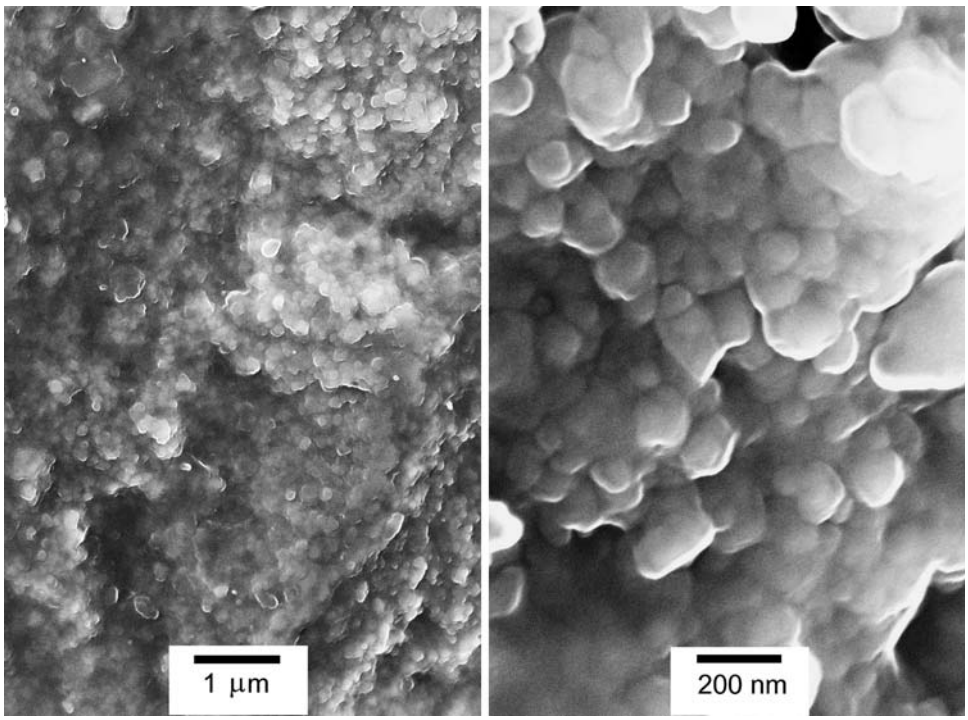

Fig. 5 SEM images of fracture surfaces of a ceramic (30 mm in diameter) made from 13 nm zirconia nanopowder doped with 2.4% Y_2O_3. Sintered at 1,150 °C for 5 min under 70 MPa

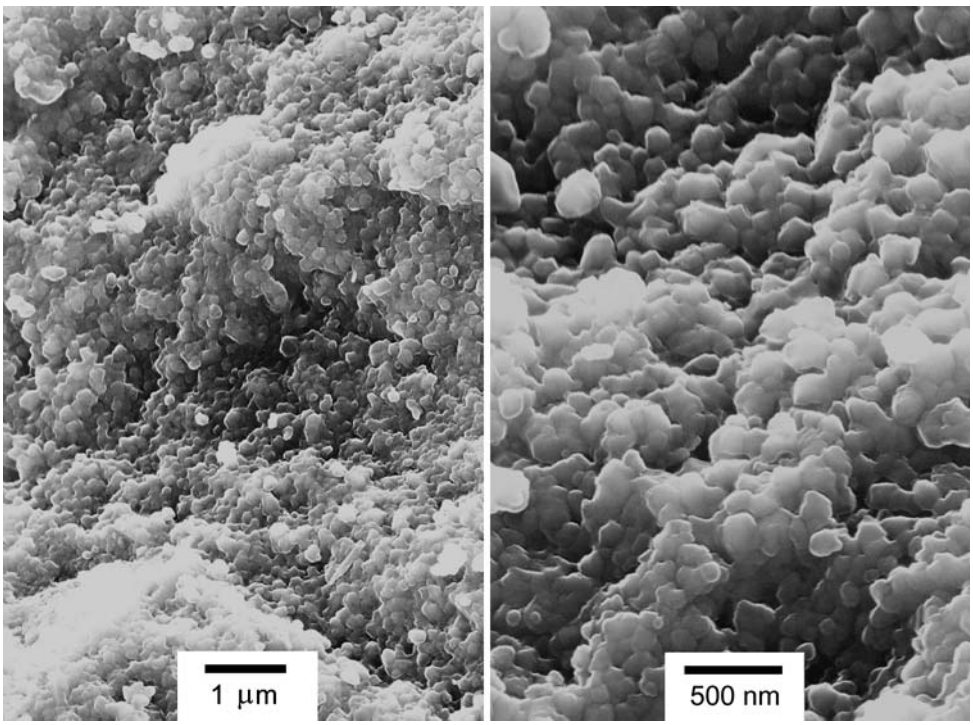

Fig. 6 SEM images of fracture surfaces of a ceramic (10 mm in diameter) made from 15 nm zirconia nanopowder doped with 9% CeO_2, 2% Al_2O_3, and 0.5% Fe_2O_3. Sintered at 1,050 °C for 5 min under 80 MPa

including those listed in Table 1. The data points denoted by filled symbols are for ceramics prepared by SPS, and those denoted by open symbols, for ceramics prepared by consolidating the powders under a uniaxial pressure of 150 MPa followed by conventional pressureless sintering at temperatures in the range 1,100–1,200 °C for 3–8 h. It can be seen that K_{IC} and H_V, varying over a wide range (depending primarily on composition), are in a tradeoff relationship; and that the ceramics prepared by SPS have superior mechanical properties to those prepared by conventional pressureless sintering.

Figure 10 shows optical micrographs of Vickers indents in (a) the Ce-TZP made from the C-powder and (b) one of the Y-TZPs made from the Y-powder, both by SPS. In the

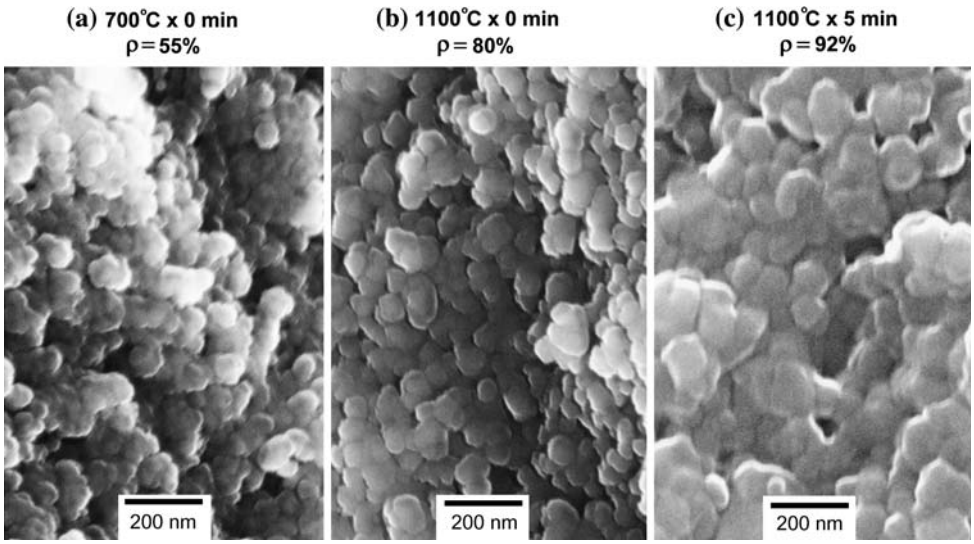

Fig. 7 SEM images of fracture surfaces of ceramics made from 12 nm zirconia nanopowder doped with 4% CeO_2 and 1% Y_2O_3. Sintered under 50 MPa

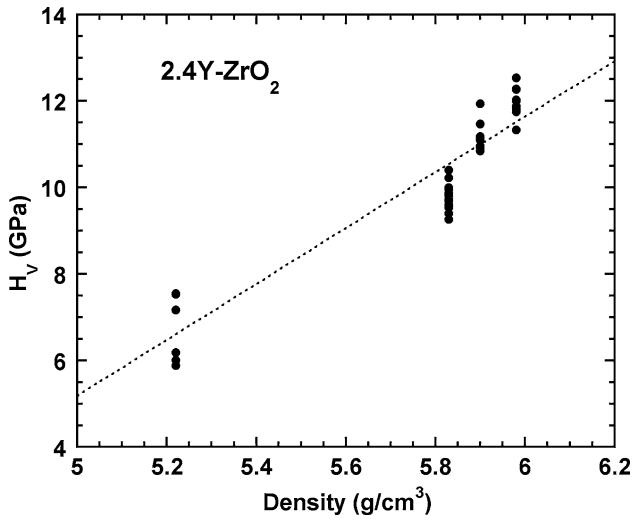

Fig. 8 Variation of Vickers hardness with density in ceramics made from Y_2O_3-doped zirconia nanopowders

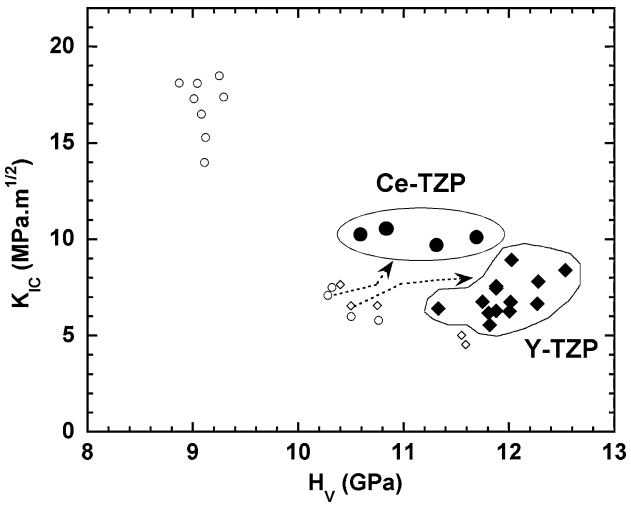

Fig. 9 Fracture toughness versus hardness relationship for nearly fully dense ceramics made from MCP zirconia nanopowders. Filled symbols: ceramics prepared by SPS. Open symbols: ceramics prepared by conventional pressureless sintering (powders consolidated under 150 MPa and sintered at 1,100–1,200 °C for 3–8 h). Circles (●, ○) and diamonds (◆, ◇) indicate Ce- and Y- TZPs, respectively

Ce-TZP, the cracks around the indent are very short, corresponding to high K_{IC}. A round pit is observed around the indent, demonstrating that plastic deformation occurred under the load as a result of stress-induced tetragonal-to-monoclinic phase transformation. This is a clear indication that the high K_{IC} is due to the transformation toughening effect. In the Y-TZP, the indent is smaller and the cracks are longer than in the Ce-TZP, corresponding to higher H_V and lower K_{IC}. Plastic deformation around the indent is still evident, although it is not as prominent as in the Ce-TZP.

As demonstrated in this and previous work [7], MCP zirconia nanopowders are unique in that they can be sintered to near full density at low temperature even when only a moderate uniaxial pressure is used for powder consolidation (in the case of conventional sintering) or during SPS.

We believe there are two major factors contributing to the high sinterability of the MCP powders: (1) the absence of hard agglomeration and (2) spherical particle morphology. The first feature results from the fact that in MCP the nanoparticles formed during heat treatment are separated by a diluent phase; spatial separation of nanoparticles using a second phase is central to MCP. The second feature stems from the fact that in MCP there is no milling step involved after nanoparticles are formed. These features are difficult to achieve in nanopowder synthesis by conventional methods such as coprecipitation and hydrolysis, since the calcination of precursor materials, needed to form

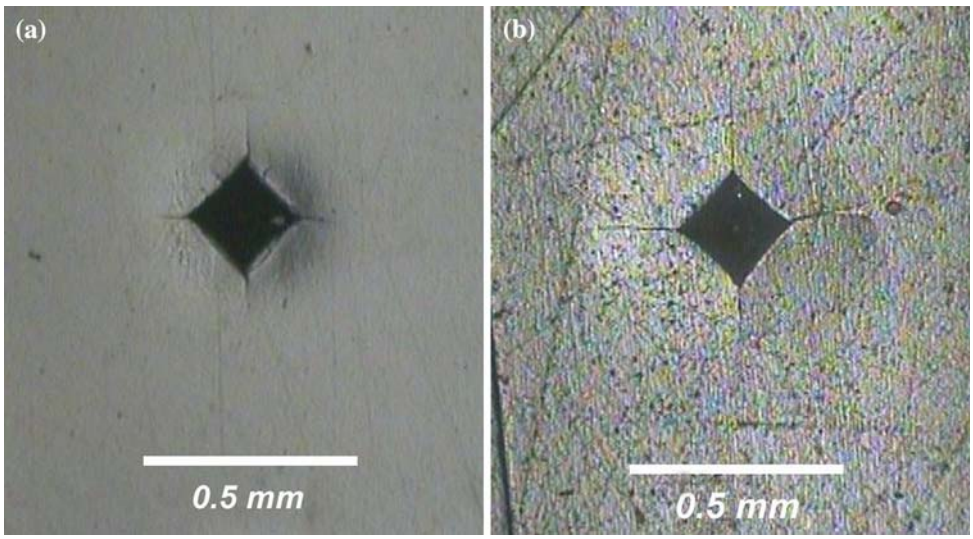

Fig. 10 Optical micrographs of Vickers indents in (**a**) Ce-TZP and (**b**) Y-TZP, both prepared by SPS

crystalline zirconia, generally leads to aggregates of primary particles, which have to be ground down afterward. Thus, the resultant particles tend to have fracture surfaces and irregular morphology.

Let us consider the final stage of powder preparation by MCP: the recovery of a powder from nanoparticle dispersion. The first step is to induce particle flocculation, which is achieved by bringing the pH near the isoelectric point. The supernatant is then discarded, and the precipitate dried into powder. The process of particle flocculation and drying (process I) is illustrated schematically to the left of Fig. 11a. During flocculation, the particles will rearrange themselves so that each particle has as many nearest neighbors as possible, thereby minimizing the potential energy associated with Van der Waals attraction. Such rearrangement is possible, since the particles are near spherical and are free to roll over adjacent ones. As a consequence, the dried powder consists of spherical primary particles densely packed into weak agglomerates (see Fig. 2). This kind of agglomerate is easy to deform under pressure, since the constituent particles can rearrange themselves through rotation and sliding, which are easy for spherical particles. Thus, only a moderate pressure is needed to press the powder into a homogeneous green body having no macroscopic pores [process II in Fig. 11a].

By contrast, conventional nanoparticles are not free to roll over adjacent ones because of irregular morphology. The resultant powder thus consists of loose agglomerates having intra-agglomerate pores [process I in Fig. 11b]. The intra-agglomerate pores are difficult to collapse during pressing

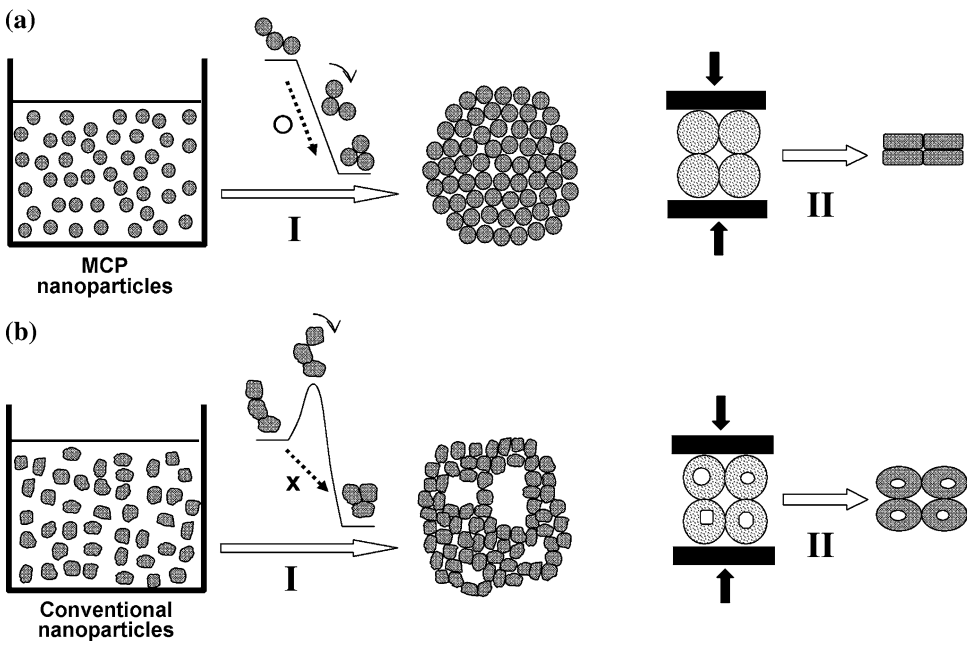

Fig. 11 Schematic diagrams illustrating (I) the process of nanoparticle flocculation and drying and (II) the process of powder pressing

because of the arching effect. Inter-agglomerate pores are also difficult to eliminate, since the deformation of agglomerates through particle rotation and sliding is difficult because of irregular particle morphology. Thus, a homogeneous green body, necessary for low-temperature sintering, cannot be formed under a moderate pressure. The process of pressing is illustrated schematically to the right of Fig. 11b.

To further demonstrate the uniqueness of the MCP powder, we have made pore-size analysis of pressed pellets by means of nitrogen absorption. The sample pellets were prepared by pressing an MCP powder and a conventional nanopowder (synthesized by a standard coprecipitation method) under a moderate pressure of 150 MPa. The results are presented in Fig. 12. For the MCP powder the pore size is comparable to the primary particle size (~15 nm), and there are no pores greater than about 40 nm. Furthermore, the cumulative pore volume is essentially the same as the pore volume determined from the density, thus ruling out the possibility that larger pores exist outside the measurement range. Since the pellet is homogeneous on a microscopic scale, it can be sintered to full density at low temperature. For the conventional nanopowder, on the other hand, some pores are much greater than the primary particle size (~7 nm). Moreover, the cumulative pore volume is considerably smaller than the pore volume determined from the density, indicating the presence of larger pores outside the measurement range. Containing large pores, this kind of pellet cannot be sintered to full density at low temperature.

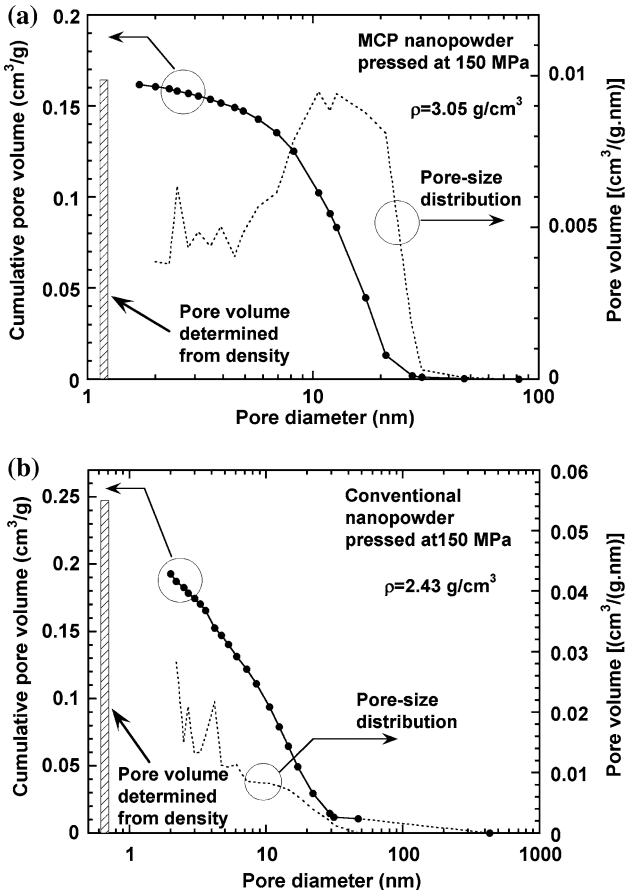

Fig. 12 Results of pore-size analysis of pressed pellets made of (**a**) CeO_2-doped MCP zirconia nanopowder and (**b**) conventional nanopowder (synthesized by coprecipitation) having the same composition. The sample pellets were prepared by uniaxially pressing the powders under 150 MPa. The hatched bar to the left indicates the specific pore volume (V_p) determined from the bulk density of the pellet using the formula $V_p = (1/\rho_b) - (1/\rho_0)$, where ρ_b and ρ_0 are the bulk density of the pellet and the density of zirconia, respectively

Apart from high sinterability, MCP zirconia nanopowders have additional advantages over conventional nanopowders:

(1) MCP powders are not fluffy, and have a high tap density comparable to that of commercial sub-micron powders, thus making die or mold filling easier. This is particularly important when the production line is automated or when a three-dimensional object, like a blasting nozzle, is to be prepared by SPS.
(2) MCP powders exhibit much smaller elastic spring-back during ejection from the die after pressing than conventional nanopowders, thus allowing the preparation of larger green bodies by dry pressing.
(3) Pressed under a given pressure, MCP powders lead to a considerably higher green density. In the case of the pellets used for the pore-size analysis (pressed under 150 MPa), the green density for the MCP powder (3.05 g/cm^3) was 20% higher than that for the powder prepared by a coprecipitation method (2.43 g/cm^3). The former value was even higher than that for a commercial sub-micron powder (Z Tech SYP Ultra), 2.95 g/cm^3. A higher green density translates into a smaller shrinkage during sintering, which on the one hand allows a more precise dimensional control of the sintered article and on the other reduces the risk of cracking due to differential shrinkage resulting from temperature gradients.

We believe that all these advantages, as well as high sinterability, result from the fact that the MCP zirconia nanopowders consist of pseudo-spherical primary particles densely packed into weak agglomerates. In a sense, the powders are appropriately granulated as prepared.

Conclusions

In this work Ce- and/or Y-doped zirconia nanopowders have been synthesized by a two-step process, consisting of the preparation of undoped zirconia particles by MCP followed by the addition of a stabilizing agent by precipitation. The

powders thus synthesized consisted of pseudo-spherical primary particles densely packed into weak agglomerates.

Using these powders, partially stabilized zirconia ceramics having near full density and a grain size of around 100 nm have successfully been prepared by SPS at low temperatures (1,050–1,150 °C) under moderate pressures (50–80 MPa). These temperatures and pressures are much lower than those required to prepare high-density ceramics from conventional zirconia nanopowders by SPS.

Measurements of H_V and K_{IC} showed that the ceramics prepared by SPS had superior mechanical properties to those prepared by pressureless sintering. The H_V and K_{IC} of zirconia ceramics vary over a wide range, depending primarily on composition, but for a given powder the use of SPS instead of pressureless sintering was found to improve H_V or K_{IC}, or both.

It is argued that the high sinterability of the MCP nanopowders is ascribed to their ability to form uniform powder compacts under relatively low pressure, and that that ability in turn originates in two features of the MCP powders: absence of hard agglomeration and pseudo-spherical particle morphology.

The high sinterability and the superior mechanical properties of sintered ceramics, combined with other advantages such as high tap density and high compactibility, make the powders particularly suitable for use in the fast, near net shape production of zirconia ceramics by SPS.

References

1. Rhodes WH (1981) J Am Ceram Soc 64:19
2. Skandan G (1995) NanoStruct Mater 5:111
3. Sardic V, Winterer M, Hahn H (2000) J Am Ceram Soc 83:729
4. Gao L, Lia W, Wanga HZ, Zhoub JX, Chaob ZJ, Zaib QZ (2001) J Eur Ceram Soc 83:135
5. Bravo-Leon A, Morikawa Y, Kawahara M, Mayo MJ (2002) Acta Mater 50:4555
6. Mayo MJ, Suresh A, Porter WD (2003) Rev Adv Mater Sci 5:100
7. Muroi M, Trotter G (2006) Ceramic Trans 190:129 [Also in Proceedings of the 6th pacific rim conference on ceramic and glass technology, Maui, Hawaii, September 2005 (in CD-ROM).]
8. McCormick PG, Ding J, Miao W–F, Street R (2001) US Patent 6203768 B1
9. McCormick PG, Tsuzuki T (2003) US Patent 6503475
10. Ding J, Tsuzuki T, McCormick PG, Street R (1996) J Phys D—Appl Phys 29:2365
11. Ding J, Tsuzuki T, McCormick PG (1996) J Am Ceram Soc 79:2956
12. Dodd AC, Raviprasad K, McCormick PG (2001) Scripta Mater 44:689
13. Dodd AC, McCormick PG (2001) Acta Mater 49:4215
14. Dodd AC, McCormick PG (2002) J Eur Ceram Soc 22:1823
15. Tsuzuki T, McCormick PG (1997) Appl Phys A 65:607
16. Liu W, McCormick PG (1999) NanoStruct Mater 12:187
17. Muroi M, Street R, McCormick PG (2000) J Appl Phys 87:3424
18. Muroi M, Street R, McCormick PG, Amighian J (2001) Phys Rev B 63:184414
19. Yoshimura M, Ohji T, Sando M, Niihara K (1988) J Mater Sci Lett 17:1389
20. Li W, Gao L (2000) J Eur Ceram Soc 20:2441
21. Chen XJ, Khor KA, Chan SH, Yu LG (2003) Mater Sci Eng A341:43
22. Anselmi-Tamburini U, Garay JE, Munir ZA, Tacca A, Maglia F, Spinolo G (2004) J Mater Res 19:3255
23. Anselmi-Tamburini U, Garay JE, Munir ZA (2006) Scripta Mater 54:823
24. Graeve OA, Singh H, Clifton A (2005) In: Proceedings of the 6th pacific rim conference on ceramic and glass technology, Maui, Hawaii, September 2005 (in CD-ROM)
25. Amin KE (1991) Toughness, hardness, and wear. In: Schneider SJ (ed) Ceramics and glasses, engineering materials handbook, vol 4. ASM International, Materials Park, p 601